Suspension models for testing shape similarity methods

Marc Ethier[2,1] and Tomasz Kaczynski[1*]
[1]Université de Sherbrooke
[2]Uniwersytet Jagielloński

December 19, 2013

Abstract

A model based on the concept of topological suspension is constructed with the purpose of testing and comparing different shape similarity measures in computer vision and graphics. This model gives an automatic way to produce interesting shapes of arbitrarily high dimension as quality tests of algorithms that have been used in low dimensions, but are now intended for comparing multidimensional data sets. The analysis of the matching distance method is provided for one and two-parameter measuring functions on closed curves and surfaces, whose suspension is defined, respectively, on surfaces in $\mathbb{R}^3$ and 3D objects in $\mathbb{R}^4$. Perspectives for applying this model to other shape descriptors used for digital images are pointed out.

Keywords: Topological suspension; shape similarity; persistent homology; filtration; matching distance

1 Introduction

In this paper, we present a model based on the concept of topological suspension for testing and comparing different shape similarity measures. This model shall give an automatic way to produce interesting shapes of arbitrarily high dimension as quality tests of algorithms that have been successfully used in the lowest dimensions, but are now intended for comparing multidimensional data sets. Data of arbitrarily high dimension arise in computational dynamics, in particular in PDEs of evolutionary type as a result of Fourier series projection or of discretization of the space variable. See, for example, [8, 16, 12] and references therein. Another example of high-dimensional data comes from considering the time index in streams of images as an additional dimension. In this way a stream of 2D images can be interpreted as a 3D image [17, 20]. One of the authors of [20] is currently working on applying this principle to pattern analysis of streams of 3D images interpreted as 4D images. Such data may be huge and thus numerically

*Supported by the NSERC of Canada discovery grant

challenging, but since we do not know a priori the expected output of the topology algorithm, we cannot be sure if it gives the right results. Hence, unless the data and its structure is already well-known, it may not be suitable for testing. Conversely, high-dimension examples constructed by hand are typically not very demanding from a numerical standpoint. The suspension process allows the construction of models with the desired topological characteristics in any dimension.

Let us outline this procedure which will be presented in detail in Section 2. Let M be an n-dimensional triangulated manifold representing a given shape, and let f be a continuous function on M with values in $\mathbb{R}$ which measures a feature of interest of M. In papers on applications to shape comparison such a function is called *measuring function* (e.g. [11]), and is often interpolated from its values on vertices of a given mesh.

The topological descriptor of shapes we will focus our attention on is the homology rank invariant, one of many ways of measuring how the topology of the sublevel set changes as we pass through a critical value of the function f. This shape descriptor permits measuring the *persistence* or, in other words, the robustness of homology generators, thus distinguishing those which may appear due to noise in the data from structural ones. The term *rank invariant* was perhaps first introduced in [4] in the context of multidimensional persistence, but in case of one-dimensional persistence, the information given by the rank invariant can be graphically displayed in two equivalent ways: either as the *persistence diagram* [9] or as a *barcode* [5]. Given two different shapes M and N, and their measuring functions f and g, a distance between rank invariants is a measure of similarity between the shapes. We focused our attention on the *matching distance* [11] but our model carries over to any other known distance with the stability property, for instance, to the *Wasserstein distance* [10].

We construct a measuring function $S_1 f$ on the topological suspension SM, also with values in $\mathbb{R}$, and with the property that its rank invariants are basically those of f with the homology dimension q shifted by one (Theorem 2.3). In particular, the 0-dimensional rank invariant, also called the *size function* [15, 23] of $S_1 f$ is quasi-trivial, and the one-dimensional rank invariant of $S_1 f$ provides about the same information as the size function of f. Note that by iterating this construction, we can produce shapes of arbitrary dimensionality whose interesting features are shifted to the highest dimension.

Our next result is Theorem 2.5 showing the relation between the matching distances of two measuring functions and their suspensions. We then extend the construction to suspensions $S_k f$ of multiparameter functions $f : M \to \mathbb{R}^k$, also called multidimensional measuring functions. The multidimensional persistent homology was first introduced in [4] in the context of discrete filtrations. Its motivation is that a multifiltration may detect geometric features which separate k coordinate-wise tests cannot detect. Multidimensional 0th order rank invariants were first applied to the shape similarity analysis based on continuous measuring functions in [3]. A bridge between the discrete and continuous settings is established in [6].

Our construction was motivated by the fact that current numerical ex-

perimentation seems to suggest that in some cases, shape comparison using homology rank invariants can be reduced in practice to that of multidimensional 0th order rank invariants provided the dimension of the parameter space is increased. Our goal is not to object to this experimental assertion, but rather to indicate that the exchange of the method cannot be done blindly, that is, without knowing the shape of the object we want to study, and that it may induce a higher computational cost than computing rank invariants for higher homology dimensions.

In Section 3, the analysis of the matching distance method is provided for two-parameter measuring functions on closed curves and surfaces, whose suspension is defined, respectively, on surfaces and on 3D objects in 4D space.

In Section 4, perspectives for applying our construction to other known shape descriptors in digital imaging are suggested. We give two examples: one is the Morse descriptor introduced in [1] and another one is the method of image matching by transformation maps introduced in [13]. In applications to digital imaging, where pixels and voxels are of concern, cubical grids are the most convenient geometric structure. However, the geometric realization of the suspension is clearly easier in simplicial meshes. Nevertheless, our model can be applied to cubical grids arising in digital imaging, by using the concept of relative homology, as we show.

Section 5 is an appendix containing the proofs of the main mathematical statements, which are our original results.

2 The model

Since the homological rank invariants are only defined for homology with coefficients in a field $\mathbb{F}$, we will use the notation $H_*(X)$ for $H_*(X;\mathbb{F})$ throughout this paper.

The *suspension* of a topological space X is the quotient space $SX := X \times [-1,1]/\sim$, where $\sim$ is the identification $(x,1) \sim (y,1)$ and $(x,-1) \sim (y,-1)$ for all $x, y \in X$ [21, § 33]. This space can be visualized as a double cone over X with vertices at the parameter values $s = \pm 1$. It is known that S is a functor on the category of topological spaces, with its value on maps $F : X \to Y$ given by $SF(x,s) := (F(x), s)$. This functor shifts the reduced homology dimension by one [21, Th. 33.2], that is

$$\tilde{H}_{q+1}(SX) \cong \tilde{H}_q(X), \ q \geq -1. \tag{1}$$

In terms of non-reduced homology, this is equivalent to writing

$$H_{q+1}(SX) \cong H_q(X), \text{ for } q \geq 1,$$

$$H_1(SX) \oplus \mathbb{F} \cong H_0(X), \text{ and } H_0(SX) \cong \mathbb{F}.$$

Let $x_0 \in X$. The *based suspension* of the pointed space (X, x_0) is the pointed space $(\Sigma X, (x_0, 0))$, where ΣX is the quotient space of SX obtained by the additional identification $(x_0, s) \sim (x_0, 0)$ for all $s \in [-1, 1]$. Figure 1 shows an example of a topological space and its suspension.

Let us note that if X is a triangulable space, then its suspension SX is also triangulable, and given $\mathcal{K}$ a triangulation of X we can construct $S(\mathcal{K})$, also called the *suspension* of the complex $\mathcal{K}$, as the join $S(\mathcal{K}) = \mathcal{K} \star \{w_0, w_1\}$, where $\{w_0, w_1\}$ is a complex composed of two vertices. That is, the simplices of $S(\mathcal{K})$ are composed of every simplex $[a_0, a_1, \ldots, a_n]$ of $\mathcal{K}$, as well as $[w_0, a_0, a_1, \ldots, a_n]$ and $[w_1, a_0, a_1, \ldots, a_n]$. The suspension $S(\mathcal{K})$ can be seen as the union of two cones over $\mathcal{K}$, and if $\mathcal{K}$ is a triangulation of X, then $S(\mathcal{K})$ is also a triangulation of SX. In this case, it is known that ΣX is homotopy equivalent to SX [18, § 4.3].

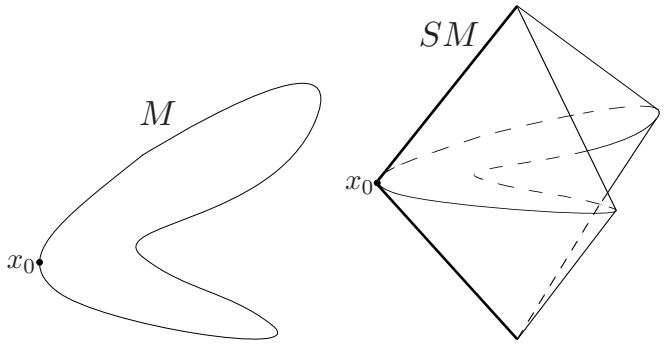

Figure 1: Left: a manifold M homeomorphic to S^1, with a base point x_0 which can be interpreted as the global minimum of a measuring function. Right: the suspension SM. In the reduced suspension ΣM, the segment $\{x_0\} \times [-1, 1]$ (in bold) would additionally be reduced to a point.

We now pass to measuring functions on topological spaces. In literature on Morse theory and its applications, we usually assume that $X = M$ is a connected smooth compact manifold of dimension d and that $f : M \to \mathbb{R}$ is a *Morse function*, that is, a C^2 function whose critical points are nondegenerate and have distinct critical values. Among other consequences, this hypothesis permits the definition of the *Morse index* of a critical point p of f as the dimension of the negative eigenspace of the Hessian matrix of f at p. However, in this paper we will only assume that f is of class C^1 unless otherwise stated. Let m_0 be the global minimum of f attained at x_0.

Define $Ef : M \times [-1, 1] \to \mathbb{R}$ by

$$Ef(x, s) := s^2 m_0 + (1 - s^2) f(x). \tag{2}$$

Note that Ef assumes the global minimum at the union of $\{x_0\} \times [-1, 1]$ with $M \times \{-1, 1\}$. Along each line $s \mapsto (x, s)$, Ef assumes a maximum at $(x, 0)$. By simple differential calculus, we get the following statement.

Proposition 2.1. *A point (p, s) is a critical point of Ef if and only if either p is a critical point of f and $s = 0$, or $s = \pm 1$. Moreover, if p is a nondegenerate critical point of f of Morse index λ, then $(p, 0)$ is also a nondegenerate critical point of Ef of Morse index $\lambda + 1$.*

Define the maps $S_1 f : SM \to \mathbb{R}$, respectively, $\Sigma_1 f : \Sigma M \to \mathbb{R}$, as the compositions of the inverse of the quotient map of $M \times [-1, 1]$ onto SM,

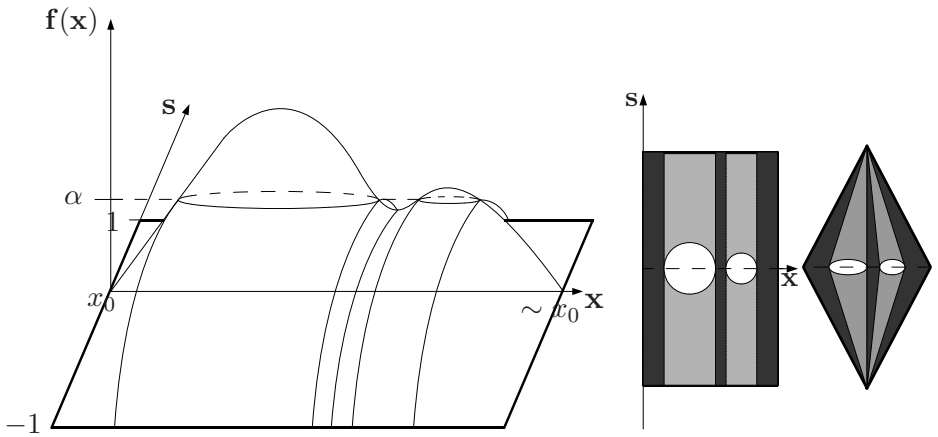

Figure 2: Left: $Ef : M \times [-1,1] \to \mathbb{R}$ for the same manifold M as in Figure 1, with end points both identified as x_0 and with measuring function $f : M \to \mathbb{R}$ reaching its global minimum in x_0. The global minimum of Ef is $(\{x_0\} \times [-1,1]) \cup (M \times \{-1,1\})$ (in bold). Middle: Ef seen from above. $E(M_\alpha)$ is in dark grey, $(EM)_\alpha$ in dark and pale grey (see Lemma 2.2). Right: $S(M_\alpha)$ is in dark grey, $(SM)_\alpha$ in dark and pale grey. $M \times \{-1\}$ and $M \times \{1\}$ are both reduced to a single point.

respectively, ΣM, with Ef. These applications are well-defined since Ef is constant on the subsets of $M \times [-1,1]$ which are sent to a point by quotient maps. The statement of Proposition 2.1 extends to $S_1 f$ except for the non-degeneracy conditions at points on $\{x_0\} \times [-1,1]$ with the critical value m_0. By passing to $\Sigma_1 f$, we gain the isolation condition for the equivalence class of $(x_0, 0)$.

Given any $\alpha \in \mathbb{R}$, we consider the sublevel sets

$$M_\alpha := \{x \in M \mid f(x) \leq \alpha\}$$

and

$$(SM)_\alpha := \{(x,s) \in SM \mid S_1 f(x,s) \leq \alpha\}.$$

It is easy to see that $S(M_\alpha) \subset (SM)_\alpha$ but the reverse inclusion does not hold true. However, the following result holds. Proof can be found in appendix, along with other long proofs of results in this article.

Lemma 2.2. *The set $S(M_\alpha)$ is homotopy equivalent to $(SM)_\alpha$.*

We now discuss the effect of the suspension operation on rank invariants. We assume that M is triangulated so that the critical points of f are vertices of the triangulation, and in particular, that x_0 is a vertex. More precisely, in practical computations, f is usually known only on vertices of a given mesh and a function f_ϵ is interpolated from f in such a way that its critical values occur only on vertices. The stability theorems [7, 6] guarantee the existence of a distance (such as the matching distance) in which the rank invariants of f and f_ϵ can be made as close as desired.

Given any $\alpha < \beta$ in $\mathbb{R}$, we consider the map

$$H_*(j^{(\alpha,\beta)}) : H_*(M_\alpha) \to H_*(M_\beta)$$

induced by the inclusion map $j^{(\alpha,\beta)} : M_\alpha \hookrightarrow M_\beta$. Recall that the q–th *persistent homology space* of (M, f) at (α, β) is the image of $H_q(M_\alpha)$ under the map $H_q(j^{(\alpha,\beta)})$ and the q–th *rank invariant* of (M, f) *at* (α, β) is the number

$$\rho_f^q(\alpha, \beta) = \operatorname{rank} \operatorname{im} H_q(j^{(\alpha,\beta)}). \tag{3}$$

The *rank invariant* function is $\rho_f^q : \Delta_+ \to \mathbb{N}$ defined on

$$\Delta_+ := \{(\alpha, \beta) \in \mathbb{R}^2 \mid \alpha < \beta\}.$$

Analogously, we define the *reduced rank invariant* function as the one on the reduced homologies:

$$\tilde{\rho}_f^q(\alpha, \beta) = \operatorname{rank} \operatorname{im} \tilde{H}_q(j^{(\alpha,\beta)}). \tag{4}$$

Here is our first result.

Theorem 2.3. *Let $f : M \to \mathbb{R}$ be a C^1 function on a connected compact manifold M. For any $(\alpha, \beta) \in \Delta_+$,*

$$\tilde{\rho}_{S_1 f}^{q+1}(\alpha, \beta) = \tilde{\rho}_f^q(\alpha, \beta), \ q \geq -1. \tag{5}$$

For the non-reduced rank invariant, we have

$$\rho_{S_1 f}^{q+1}(\alpha, \beta) = \rho_f^q(\alpha, \beta), \ q \geq 1, \tag{6}$$

$$\rho_{S_1 f}^1(\alpha, \beta) = \begin{cases} \rho_f^0(\alpha, \beta) & \text{if } \alpha < m_0, \\ \rho_f^0(\alpha, \beta) - 1 & \text{otherwise} \end{cases}, \tag{7}$$

and

$$\rho_{S_1 f}^0(\alpha, \beta) = \begin{cases} 0 & \text{if } \alpha < m_0, \\ 1 & \text{otherwise} \end{cases}. \tag{8}$$

The same formulas hold for $\Sigma_1 f$.

We can use Theorem 2.3 to prove results about the matching distance between rank invariants [11]. The previous reference discusses the use of the matching distance in size theory, which is in essence the study of the 0th rank invariant. These results can be generalized in a natural and common way to the q–th rank invariant. Recall the definition of a *cornerpoint* of the rank invariant function ρ_f:

Definition 2.4. *For a point $p = (\alpha, \beta) \in \Delta_+$, define its* multiplicity $\mu(p)$ *as the minimum, over all $\epsilon > 0$ such that $\alpha + \epsilon < \beta - \epsilon$, of*

$$\rho_f(\alpha + \epsilon, \beta - \epsilon) - \rho_f(\alpha - \epsilon, \beta - \epsilon) - \rho_f(\alpha + \epsilon, \beta + \epsilon) + \rho_f(\alpha - \epsilon, \beta + \epsilon).$$

If $\mu(p) > 0$, then p is called a proper cornerpoint *of ρ_f. In addition, for a vertical line r of equation $x = \alpha$, define its* multiplicity $\mu(r)$ *to be the minimum, over all $\epsilon > 0$ such that $\alpha + \epsilon < 1/\epsilon$, of*

$$\rho_f(\alpha + \epsilon, 1/\epsilon) - \rho_f(\alpha - \epsilon, 1/\epsilon).$$

If $\mu(r) > 0$, then r is called a cornerpoint at infinity *of ρ_f, and we identify it with the pair (α, ∞). The rank invariant function ρ_f is uniquely determined by the multiset of its cornerpoints together with their multiplicities, called its* persistence diagram *$Dgm(\rho_f)$.*

The matching distance d between the rank invariants ρ_f and ρ_g is the *bottleneck distance* between the multisets of their cornerpoints. Technical details can be found in [11, Def. 3.4-3.6] and we do not wish to encumber this article by repeating them, but generally speaking, its definition is the following:

$$d(\rho_f, \rho_g) = \min_{\sigma} \max_{p \in \mathrm{Dgm}(\rho_f)} \delta(p, \sigma(p)),$$

where σ varies among the bijections between $\mathrm{Dgm}(\rho_f)$ and $\mathrm{Dgm}(\rho_g)$, and where

$$\delta((u,v),(u',v')) = \min\left\{\max\{|u-u'|, |v-v'|\}, \max\left\{\frac{v-u}{2}, \frac{v'-u'}{2}\right\}\right\}.$$

The main idea is that $d(\rho_f, \rho_g)$ is the cost of the optimal bijection moving the cornerpoints of the persistence diagram of ρ_f to those of ρ_g. However, it also recognizes that if a cornerpoint of one or both of these persistence diagrams is close to the diagonal $\Delta := \{(\alpha, \alpha) \mid \alpha \in \mathbb{R}\}$, or cannot be matched to another cornerpoint due to differing cardinalities of the diagrams, the optimal bijection might entail moving it to the diagonal. This corresponds to smoothing out small topological noise in f or g.

Theorem 2.5. *Let M, N be homeomorphic connected compact manifolds, and let $f : M \to \mathbb{R}$ and $g : N \to \mathbb{R}$ be C^1 measuring functions. Denote by m_0 and n_0 the minima, respectively, of f on M and g on N. Then*

$$d(\tilde{\rho}^{q+1}_{S_1 f}, \tilde{\rho}^{q+1}_{S_1 g}) = d(\tilde{\rho}^{q}_{f}, \tilde{\rho}^{q}_{g}), \ q \geq -1. \tag{9}$$

For the matching distance between non-reduced rank invariants:

$$d(\rho^{q+1}_{S_1 f}, \rho^{q+1}_{S_1 g}) = d(\rho^{q}_{f}, \rho^{q}_{g}), \ q \geq 1, \tag{10}$$

$$d(\rho^{1}_{S_1 f}, \rho^{1}_{S_1 g}) \leq d(\rho^{0}_{f}, \rho^{0}_{g}), \tag{11}$$

and

$$d(\rho^{0}_{S_1 f}, \rho^{0}_{S_1 g}) = |m_0 - n_0|. \tag{12}$$

Furthermore, if $m_0 = n_0$, then we have

$$d(\rho^{q+1}_{S_1 f}, \rho^{q+1}_{S_1 g}) = \begin{cases} d(\rho^{q}_{f}, \rho^{q}_{g}) & \text{if } q \geq 0, \\ 0 & \text{if } q = -1 \end{cases}. \tag{13}$$

The same formulas hold for $\Sigma_1 f$ and $\Sigma_1 g$.

From this point on, let us consider simplicial complexes $\mathcal{K}$ and $\mathcal{L}$, assumed to be the triangulations of homeomorphic compact connected manifolds M and N. We equip these complexes with k-dimensional measuring functions $\varphi : \mathcal{V}(\mathcal{K}) \to \mathbb{R}^k$ and $\psi : \mathcal{V}(\mathcal{L}) \to \mathbb{R}^k$, where $\mathcal{V}$ refers to the vertex

set of the complex under consideration. The functions may be obtained by sampling measuring functions $f : M \to \mathbb{R}^k$ and $g : N \to \mathbb{R}^k$ of class C^1. For a complex $\mathcal{K}$ equipped with a measuring function $\varphi : \mathcal{V}(\mathcal{K}) \to \mathbb{R}^k$, and a value $\alpha \in \mathbb{R}^k$ we further define the sublevel complex $\mathcal{K}_\alpha$ as the complex composed of all simplices of $\mathcal{K}$ whose vertices v all verify the relation $\varphi(v) \preceq \alpha$, where $\preceq$ is the usual partial order on $\mathbb{R}^k$. We shall define, for $\varphi : \mathcal{V}(\mathcal{K}) \to \mathbb{R}^k$, the measuring function $S_k\varphi = (S_1\varphi_1, \ldots, S_1\varphi_k) : \mathcal{V}(S(\mathcal{K})) \to \mathbb{R}^k$ on the vertices of the suspension $S(\mathcal{K}) = \mathcal{K} \star \{w_0, w_1\}$, where $S_1\varphi_i(v) = \varphi_i(v)$ for all vertices v of $\mathcal{K}$, and $S_1\varphi_i(w_j) = m_{i,0}$, $j = 0, 1$, $m_{i,0}$ being the absolute minimum of φ_i over $\mathcal{V}(\mathcal{K})$.

We can define the rank invariants for the discrete model. Consider the map

$$H_*(j^{(\alpha,\beta)}) : H_*(K_\alpha) \to H_*(K_\beta)$$

induced by the inclusion map $j^{(\alpha,\beta)} : K_\alpha \hookrightarrow K_\beta$, where $\alpha \prec \beta$ and where K_α and K_β denote the supports of the sublevel complexes $\mathcal{K}_\alpha$ and $\mathcal{K}_\beta$. We define the q–th rank invariant of (K, φ) at (α, β) to be

$$\rho^q_\varphi(\alpha, \beta) = \operatorname{rank} \operatorname{im} H_q(j^{(\alpha,\beta)}).$$

As proved in [6], the rank invariant functions ρ_φ are identical to the rank invariant functions $\rho_{\varphi^\urcorner}$, where $\varphi^\urcorner : K \to \mathbb{R}^k$ is the axis-wise interpolation of φ.

In [3] a foliation method was introduced to reduce the computation of multidimensional rank invariants to that of a parametrized family of rank invariants for one-dimensional measuring functions. Algorithms were then developed to allow arbitrarily precise computation of the multidimensional matching distance on a finite subset of this family. In short, for every pair $(\vec{l}, \vec{b}) \in \mathbb{R}^k \times \mathbb{R}^k$ where $l_i > 0$, $\sum l_i = 1$ and $\sum b_i = 0$, called an *admissible pair* and representing a line where $\vec{l}$ is a unit direction vector oriented toward higher values in the partial order on $\mathbb{R}^k$ and where $\vec{b}$ is a starting point, we define a reduced one-dimensional measuring function on vertices as

$$\operatorname{red}^\varphi_{(\vec{l},\vec{b})}(v) = \min_{i=1,\ldots,k} l_i \max_{i=1,\ldots,k} \frac{\varphi_i(v) - b_i}{l_i}.$$

It has been shown in [3] that if $\alpha \prec \beta$ are values found on the line in $\mathbb{R}^k \times \mathbb{R}^k$ generated by $(\vec{l}, \vec{b})$, and more precisely, if $\alpha = s\vec{l} + \vec{b}$, $\beta = t\vec{l} + \vec{b}$, then we have equality of rank invariants:

$$\rho_\varphi(\alpha, \beta) = \rho_{\operatorname{red}^\varphi_{(\vec{l},\vec{b})}}(s, t).$$

This property has been used to define a k-dimensional matching distance between rank invariants:

$$D(\rho_\varphi, \rho_\psi) = \sup_{(\vec{l},\vec{b}) \in \operatorname{Adm}_k} d(\rho_{\operatorname{red}^\varphi_{(\vec{l},\vec{b})}}, \rho_{\operatorname{red}^\psi_{(\vec{l},\vec{b})}})$$

where Adm_k is the set of admissible pairs.

It should be noted that k-parameter persistence provides more information on the structure of a shape than k separate tests using single-parameter

persistence. To convince oneself of this fact, we may take a look at Figure 3. The two curves pictured cannot be distinguished by the rank invariant method using one or other of the coordinate functions. Indeed, their persistence diagrams will be identical, and the matching distance between them will be zero. However, using the reduction method, we find directions where topological properties are not born at the same point for both curves. We can therefore conclude that the 2-dimensional matching distance between their rank invariants will be positive.

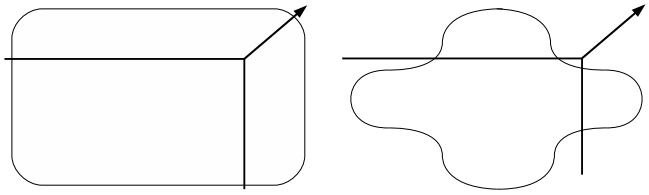

Figure 3: Two curves in $\mathbb{R}^2$. We consider as measuring functions the coordinate functions. The arrow is a direction corresponding to an admissible pair of Adm_2, while the lines represent a level set of the reduced function. We see that, at the value of interest, the sublevel set for the second curve has two connected components, while that for the first one has a single connected component. The persistence diagrams for the reduced function will therefore be different.

Theorem 2.6. *Let $\mathcal{K}$, $\mathcal{L}$ be simplicial complexes, and let $\varphi : \mathcal{V}(\mathcal{K}) \to \mathbb{R}^k$ and $\psi : \mathcal{V}(\mathcal{L}) \to \mathbb{R}^k$ be k-dimensional measuring functions. Then*

$$D(\tilde{\rho}^{q+1}_{S_k\varphi}, \tilde{\rho}^{q+1}_{S_k\psi}) = D(\tilde{\rho}^{q}_{\varphi}, \tilde{\rho}^{q}_{\psi}),\ q \geq 0. \tag{14}$$

For the k-dimensional matching distance between non-reduced rank invariants:

$$D(\rho^{q+1}_{S_k\varphi}, \rho^{q+1}_{S_k\psi}) = D(\rho^{q}_{\varphi}, \rho^{q}_{\psi}),\ q \geq 1, \tag{15}$$

and

$$D(\rho^{1}_{S_k\varphi}, \rho^{1}_{S_k\psi}) \leq D(\rho^{0}_{\varphi}, \rho^{0}_{\psi}). \tag{16}$$

Remark 2.7. We believe that Theorem 2.6 is probably also true in the continuous case, that is, with manifolds M, N equipped with continuous measuring functions $f : M \to \mathbb{R}^k$ and $g : N \to \mathbb{R}^k$. However, the proof appears to be more complicated in this case. Since our interest is in the numerics, assuming the simplicial framework was sufficient.

3 Numerical examples

The numerical examples described in this section have been produced with two-dimensional measuring functions. In this case, we note that the set of admissible pairs Adm_2 is the set of pairs $((a, 1-a), (b, -b))$ where $a \in (0, 1)$ and $b \in \mathbb{R}$. For a measuring function $\varphi : \mathcal{V}(\mathcal{K}) \to \mathbb{R}^2$, we will denote the reduced one-dimensional functions $\mathrm{red}^{\varphi}_{((a,1-a),(b,-b))}$ by $\Phi_{(a,b)}$, and

$\mathrm{red}^{S_2\varphi}_{((a,1-a),(b,-b))}$ as $\mathbb{S}_2\Phi_{(a,b)}$. Our examples are intended to provide experimental support for the theory described in the previous section. We have used two pairs of models, each of which are 1 or 2-dimensional simplicial complexes homeomorphic to connected and compact manifolds, as well as their simplicial suspensions as previously defined.

We have used an implementation of the algorithm of [2] to compute lower bounds for the two-dimensional matching distance between their rank invariants of various orders with decreasing error tolerance. This algorithm, given pairs (X, φ) and (Y, ψ), computes $d(\rho_{\Phi_{(a,b)}}, \rho_{\Psi_{(a,b)}})$, with (a, b) chosen on increasingly fine grids, until the desired tolerance ϵ, that is, the worst case error between the computed and exact 2-dimensional matching distances, is attained. Its total complexity depends on the complexity of the persistence and one-dimensional matching distance algorithms. It is known that computing persistent homology has complexity $O(m^3)$ in the worst case, where m is the number of simplices in the complex [24]. The complexity of one-dimensional matching distance computation is $O(p^{2.5})$, where p is the maximal number of cornerpoints allowed [11]. The grid algorithm of [2] requires in the worst case a number of computations proportional to $1/\epsilon^2$, representing the number of grid points. Our implementation (coded in Java with help from N. Cavazza, co-author of [6] along with this paper's authors) computes the persistence diagrams for these rank invariants using the persistent homology software JPlex [22]. In addition, constructing the suspension of a simplicial complex is linear on the number of simplices of the original complex.

Example 3.1. The contour model example is the pair of models (K, φ) and (L, ψ) shown in Figure 4, along with the persistence diagrams for $\rho^0_{\varphi_2}$ and $\rho^0_{\psi_2}$. Its suspension is a two-dimensional simplicial complex embedded in $\mathbb{R}^3$; sort of a simplicial version of the curve and surface seen in Figure 1. As shown, both φ_1 and ψ_1, and φ_2 and ψ_2, take the same global minimum (in both cases 0), so we expect Equation (13) to hold. The 2D matching distances have been computed with a tolerance $\epsilon = 0.01$, but given the simplicity of the example their exactness is easy to show. The results of our computations can be found in the following two tables:

	ρ	$\tilde{\rho}$
$d(\rho^0_{\varphi_1}, \rho^0_{\psi_1})$	0.05	0.05
$d(\rho^0_{\varphi_2}, \rho^0_{\psi_2})$	0.15	0.15
$D(\rho^0_{\varphi}, \rho^0_{\psi})$	0.2	0.15

	$q=0$	$q=1$
$d(\rho^q_{S_1\varphi_1}, \rho^q_{S_1\psi_1})$	0	0.05
$d(\rho^q_{S_1\varphi_2}, \rho^q_{S_1\psi_2})$	0	0.15
$D(\rho^q_{S_2\varphi}, \rho^q_{S_2\psi})$	0.1	0.15

As seen above, $D(\rho^0_{S_2\varphi}, \rho^0_{S_2\psi})$ cannot be assumed to equal 0, even if φ_i and ψ_i take the same global minimum for $i = 1, 2$. We haven't included the results for the reduced rank invariants for the suspended models, since they are equal to that of the non-reduced rank invariants. This isn't however expected to be true in general. Figure 5 further shows $d(\rho^q_{\Phi_{(a,b)}}, \rho^q_{\Psi_{(a,b)}})$ and $d(\rho^q_{\mathbb{S}_2\Phi_{(a,b)}}, \rho^q_{\mathbb{S}_2\Psi_{(a,b)}})$ plotted in function of a and b, for a few interesting choices of q.

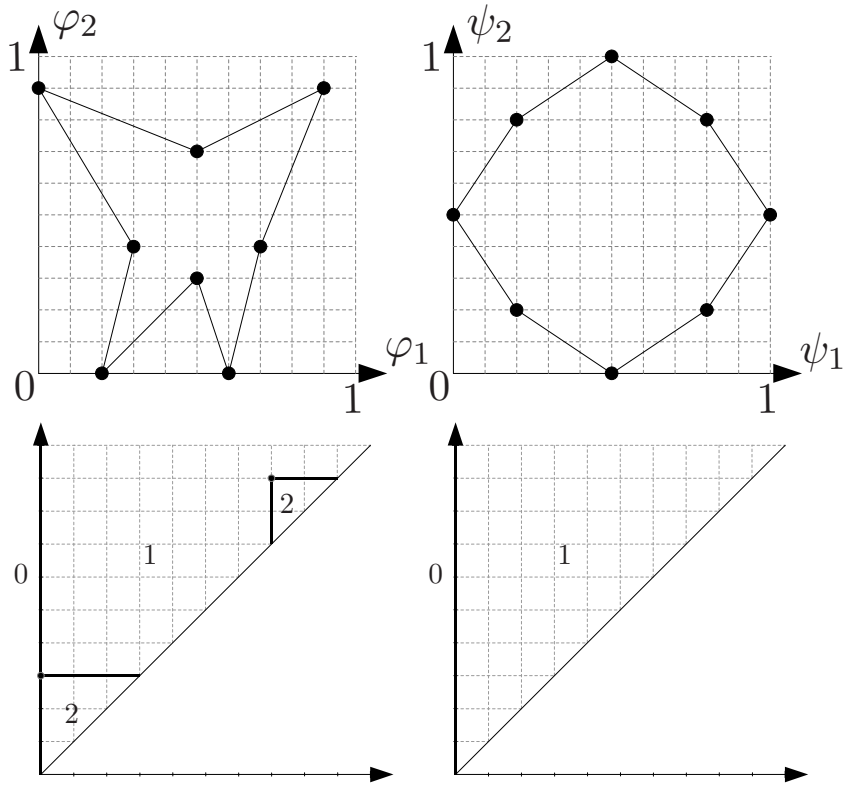

Figure 4: Top row: pair of models for the contour model example. The measuring functions are the x and y coordinate functions. Bottom row: persistence diagrams for the rank invariant functions $\rho^0_{\varphi_2}$ and $\rho^0_{\psi_2}$. First function has one cornerpoint at infinity (bold line at $(0, \infty)$) and two proper cornerpoints (marked points at $(0, 0.3)$ and $(0.7, 0.9)$), second function has only one cornerpoint at infinity at $(0, \infty)$. Matching distance is 0.15, that is, cost of moving cornerpoint $(0, 0.3)$ onto Δ. Numbers represent the value of the rank invariant function on subsets of Δ_+.

Example 3.2. The surface mesh model is shown in Figure 6. Its suspension is a three-dimensional simplicial complex embedded in $\mathbb{R}^4$, which cannot be accurately shown without playing a video with the fourth dimension mapped to time. The measuring function $\varphi : \mathcal{V}(\mathcal{K}) \to \mathbb{R}^2$ is defined in the following way: assuming that $\mathcal{V}(\mathcal{K}) = \{v_1, \ldots, v_n\}$ and that c is the centre of mass of K defined by taking the weighted average of the centres of each triangle, we define the principal vector

$$\vec{w} = \frac{\sum_{i=1}^{n} (v_i - c)\|v_i - c\|_2}{\sum_{i=1}^{n} \|v_i - c\|_2^2}$$

where $\|\cdot\|_2$ refers to the Euclidean norm. Then, let d be the line passing through c having $\vec{w}$ as direction vector, and π be the plane passing through c having $\vec{w}$ as normal vector. The function φ is defined as

$$\varphi_1(v_i) = 1 - \frac{\operatorname{dist}(v_i, d)}{\max_{j=1,\ldots,n} \operatorname{dist}(v_j, d)}$$

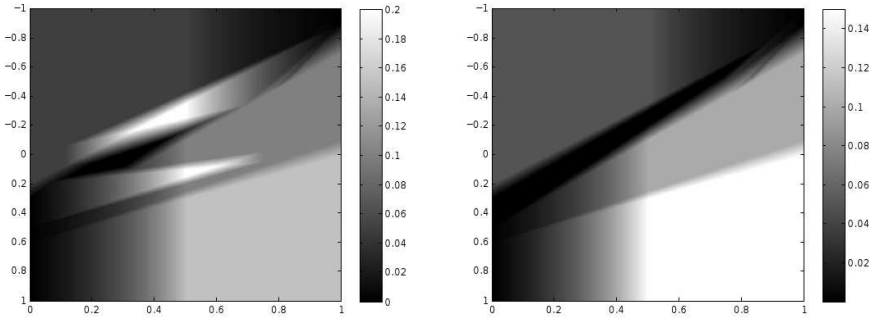

Figure 5: First image: plot of $d(\rho^0_{\Phi_{(a,b)}}, \rho^0_{\Psi_{(a,b)}})$. Second image: plot of $d(\tilde{\rho}^0_{\Phi_{(a,b)}}, \tilde{\rho}^0_{\Psi_{(a,b)}})$ and $d(\rho^1_{\mathbb{S}_2\Phi_{(a,b)}}, \rho^1_{\mathbb{S}_2\Psi_{(a,b)}})$. They are identical, as expected by Equation (9). Horizontal axis is a, vertical axis is b.

and

$$\varphi_2(v_i) = 1 - \frac{\operatorname{dist}(v_i, \pi)}{\max_{j=1,\ldots,n} \operatorname{dist}(v_j, \pi)},$$

where dist refers to the Euclidean distance between a point and the line d or plane π. The measuring function ψ is defined equivalently on the vertex set $\mathcal{V}(\mathcal{L})$. By the definition of the measuring functions, the absolute minima of φ_1, φ_2, ψ_1 and ψ_2 will all be 0. Table 1 shows the results of our computations. All lower bounds for the 2D matching distance are shown, in order to illustrate the comparability of results between the original and suspended models at every step in the algorithm.

4 Perspectives of applications to digital images

Our focus in this paper is on the use of the topological suspension as a model in shape comparison by persistent homology methods. We finish with remarks showing that the main ideas can also be applied to many other topological methods in imaging with the same aim: to give an automatic way of producing examples of interesting shapes for providing quality tests of algorithms and programs that have been successfully used in low dimensions but which we now want to use with high-dimensional spaces. In this section we invite the readers to use their imagination in inventing similar models in their field of study, by pointing out examples of potential applications.

Our first example is the Morse descriptor introduced by [1] with the same aim as persistent homology, that is, to provide topological analysis and comparison of shapes. The authors directly apply their descriptors to digital images generated from photographs of hand gestures in a sign language, and to other digital objects. Rather than looking at the rank of inclusion maps of a lower sublevel set into an upper one, they consider an invariant based on the concept of the rank of the relative homology of one set modulo another. More precisely, the *Morse descriptor* $\mathrm{MD}_f : \Delta_+ \times \mathbb{N} \to \mathbb{N}$ is defined by

$$\mathrm{MD}_f(\alpha, \beta, q) := \operatorname{rank} H_q(M_\beta, M_\alpha).$$

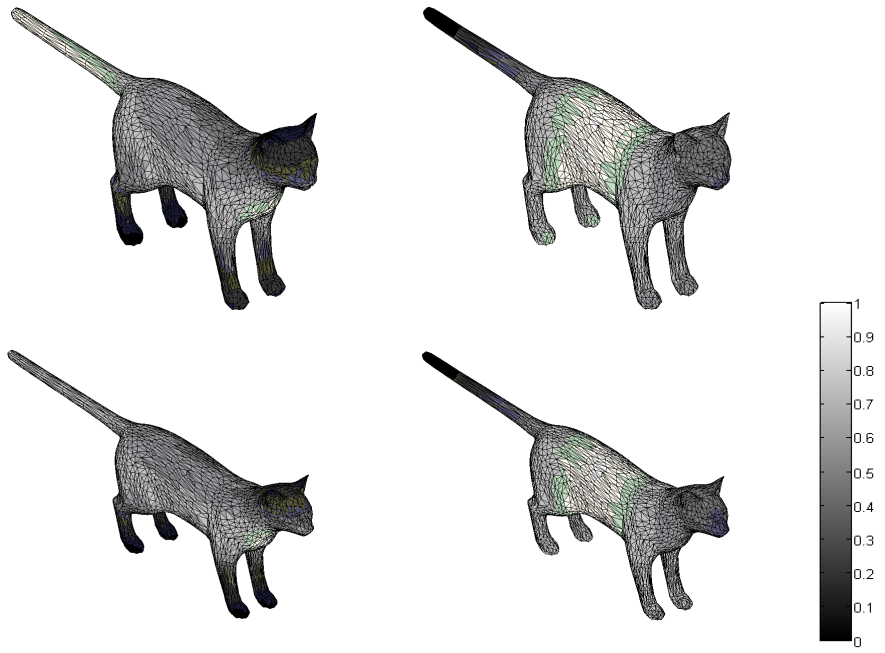

Figure 6: First row: model K along with measuring functions φ_1 and φ_2. Second row: model L along with measuring functions ψ_1 and ψ_2. Models are courtesy of the authors of [2].

This descriptor provides somewhat different information about the shape of interest than the rank invariant studied in this paper. Indeed, it focuses on the non-trivial homology cycles remaining or created in the upper level set M_β after contracting the lower level set M_α to a point, while the rank invariant focuses only on the cycles of the lower level set remaining non-trivial after immersing M_α to M_β.

We may want to investigate data of higher dimension than the initial 2D objects studied in [1] and test results on our suspension models. The suspension functor can be applied similarly as in Section 2 by the following theorem which can be proved using the relative Mayer-Vietoris sequence [21, Exercise 2 page 145] and Lemma 2.2.

Theorem 4.1. *Under the terminology of Section 2, the isomorphism*

$$H_{q+1}((SM)_\beta, (SM)_\alpha) \cong H_q(M_\beta, M_\alpha) \tag{17}$$

holds for all $q \in \mathbb{Z}$ provided that $(SM)_\alpha \neq \emptyset$. If $(SM)_\alpha = \emptyset$, (17) holds for all $q > 0$, while for $q = 0$ and $q = -1$ we have:

$$H_0(M_\beta, \emptyset) = H_0(M_\beta) \cong H_1((SM)_\beta) \oplus \mathbb{F},$$

$$H_0((SM)_\beta, \emptyset) = H_0((SM)_\beta) \cong \mathbb{F}.$$

Our next example is an image matching method presented in [13]. The method consists of estimating a transformation map between block structures (pixels, voxels, windows) of given binary images analyzed for topological correspondence, using the concept of homology of maps. The idea is

	ϵ	
$d(\rho^0_{\varphi_1}, \rho^0_{\psi_1})$		0.118165
$d(\rho^0_{\varphi_2}, \rho^0_{\psi_2})$		0.032043
$D(\rho^0_{\varphi}, \rho^0_{\psi})$	9/8	0.194217
	9/16	0.224227
	9/32	0.225394
	9/64	0.225394

	ϵ	
$d(\tilde{\rho}^0_{\varphi_1}, \tilde{\rho}^0_{\psi_1})$		0.118165
$d(\tilde{\rho}^0_{\varphi_2}, \tilde{\rho}^0_{\psi_2})$		0.032043
$D(\tilde{\rho}^0_{\varphi}, \tilde{\rho}^0_{\psi})$	9/8	0.118165
	9/16	0.127301
	9/32	0.135530
	9/64	0.144274

	ϵ	
$d(\rho^1_{\varphi_1}, \rho^1_{\psi_1})$		0.031129
$d(\rho^1_{\varphi_2}, \rho^1_{\psi_2})$		0.039497
$D(\rho^1_{\varphi}, \rho^1_{\psi})$	9/8	0.039497
	9/16	0.046150
	9/32	0.046150
	9/64	0.046150

	ϵ	
$d(\rho^1_{S_1\varphi_1}, \rho^1_{S_1\psi_1})$		0.118165
$d(\rho^1_{S_1\varphi_2}, \rho^1_{S_1\psi_2})$		0.032043
$D(\rho^1_{S_2\varphi}, \rho^1_{S_2\psi})$	9/8	0.118165
	9/16	0.127301
	9/32	0.135530
	9/64	0.144274

	ϵ	
$d(\rho^2_{S_1\varphi_1}, \rho^2_{S_1\psi_1})$		0.031129
$d(\rho^2_{S_1\varphi_2}, \rho^2_{S_1\psi_2})$		0.039497
$D(\rho^2_{S_2\varphi}, \rho^2_{S_2\psi})$	9/8	0.039497
	9/16	0.046150
	9/32	0.046150
	9/64	0.046150

	ϵ	
$d(\rho^0_{S_1\varphi_1}, \rho^0_{S_1\psi_1})$		0.000000
$d(\rho^0_{S_1\varphi_2}, \rho^0_{S_1\psi_2})$		0.000000
$D(\rho^0_{S_2\varphi}, \rho^0_{S_2\psi})$	9/8	0.155527
	9/16	0.171368
	9/32	0.179821
	9/64	0.194217

Table 1: First two tables show results for the original models with 0th order ordinary and reduced rank invariants. Third table contains results for the original models with 1st order rank invariants. Last three tables show results for the suspended models with 1st, 2nd and 0th order rank invariants. Results for suspended models with 0th order reduced rank invariants are not shown due to being similar to the sixth table. The choice of initial ϵ follows from the algorithm of [2].

to use the structure of cubical sets to represent the image data of the two compared images, respectively X and Y. One next generates the cubical chain complexes $\mathcal{C}(X)$ and $\mathcal{C}(Y)$. The authors perform experiments with three types of transformations of 2D binary images: translation, rotation, and homothety. They provide an algorithm that generates a chain map $\varphi : \mathcal{C}(X) \to \mathcal{C}(Y)$ and computes the map $H_*(\varphi)$ it induces in homology. That map carries the information on locations where important topological features (connected components or cycles) of X are carried to Y by the transformation. We believe that it is an interesting idea which has the potential of leading to algorithms for comparing shapes whose calculation time may compete with our matching distance methods.

Our model easily adapts to the described method of [13] due to the functoriality of the suspension map. Once we define the chain complexes

of the suspended images SX and SY and the suspended chain map $S\varphi : \mathcal{C}(SX) \to \mathcal{C}(SY)$, we get the homology map

$$H_*(S\varphi) : H_*(SX) \to H_*(SY).$$

The only practical issue is in suitable choice of combinatorial structures. In [13, 1, 20], and in many other works on applications of topology to digital imaging, one uses cubical sets and cubical complexes. We refer the reader to [19, Chapter 2] for a detailed presentation of those structures as well as of the cubical homology theory. There are three main reasons behind this choice. First, it is the most appropriate for representing image pixels, voxels or, more generally, n-dimensional pixels. Second, the calculation of homology based on cubical sets is by far more efficient than that based on triangulations. Third, elementary cubes have this nice property that the product of two elementary cubes is also an elementary cube of higher dimension, while the product of two simplices is not in general a simplex. However, the suspension operation is based on contracting a subset of a cylinder to a single point (a vertex of a cone), and thus it produces a polyhedral set which is no longer a cubical set. Luckily, the efficient cubical homology algorithms may still be applied by using relative homology, thus one may avoid triangulating the suspended set. In brief, the relative homology of a pair of cubical sets gives the same information as the homology of the set obtained by contracting a subset to a single point, so the actual contraction does not need to be realized in practice. The idea is illustrated by Figure 7. More explicitly, we have the isomorphism:

$$\tilde{H}_*(SX) \cong H_*(\Sigma X, [x_0]) \cong H_*(X \times [-1,1], [x_0]) \tag{18}$$

where $[x_0] = X \times \{-1,1\} \cup \{x_0\} \times [-1,1]$ is the equivalence class of the chosen base point x_0 of X under the relation defining ΣX. Given a pair of cubical sets $A \subset X$, we get

$$H_*(SX, SA) \cong H_*(\Sigma X, \Sigma A) \cong H_*(X \times [-1,1], X \times \{-1,1\} \cup A \times [-1,1]). \tag{19}$$

Similarly, one can deal with the relative homology of sublevel sets of the suspended space.

We leave up to the reader's imagination further examples of problems where our model can be applied. We also believe that other topological operations than the suspension might also be found to be of interest in imaging.

5 Appendix: Proofs of main mathematical statements

We now sketch, for the interested reader, proofs for some of the theorems we used in this paper. These proofs are original work by the authors.

Proof of Lemma 2.2 If $\alpha = m_0$ is the absolute minimum of f, then we obviously have $S(M_\alpha) = (SM)_\alpha$.

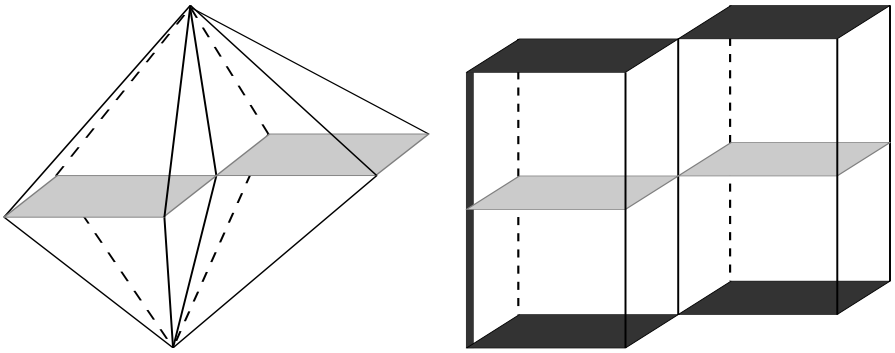

Figure 7: Left: the suspension of a cubical set (in light grey). Right: the product of this same cubical set with the interval $[-1,1]$. Assuming that the lower left vertex is the chosen base point x_0, the set $(X \times [-1,1]) \cup (\{x_0\} \times [-1,1])$ is in dark grey.

Let $EM = M \times [-1,1]$ and $(EM)_\alpha$ be the sublevel set of Ef. We first assume that α is a regular value and construct a strong deformation $h : X \times [0,1] \to X$ of the set

$$X = (EM)_\alpha \cup (M \times \{-1,1\})$$

onto

$$A = E(M_\alpha) \cup (M \times \{-1,1\}).$$

These sets are illustrated in Figure 2. Forcingly, we must have $h((x,s),\lambda) = (x,s)$ for all $(x,s) \in A$ and all $\lambda \in [0,1]$. Hence, it is enough to continuously extend h to $(X \setminus A) \times [0,1]$. By the hypothesis that α is regular, the gradient vector field $-\nabla Ef$ defines a flow $t \mapsto \varphi((x,s),t)$ on $\overline{X \setminus A}$ such that the values of Ef decrease along its trajectories. In the absence of critical points, any $(x,s) \in \overline{X \setminus A}$ is sent by φ to A in a finite time $t(x,s)$. By standard arguments from the dynamical systems theory, $t(x,s)$ is a continuous function of (x,s).

We extend h to $(X \setminus A) \times [0,1]$ by the formula

$$h((x,s),\lambda) := \varphi((x,s), \lambda t(x,s)).$$

It is easily verified that h is a strong deformation retraction of X onto A.

Since, for each λ, $h(\cdot,\lambda)$ is the identity map on $M \times \{-1,1\} \subset A$, h extends to the deformation $\tilde{h} : (SM)_\alpha \times [0,1] \to (SM)_\alpha$ by applying the quotient map. In particular, we have the homotopy equivalence $S(M_\alpha) \cong (SM)_\alpha$ for a regular value α.

Now let α be a critical value, other than the absolute minimum m_0 which is already taken care of. Since it is isolated, there exists $\epsilon > 0$ such that all values in $(\alpha, \alpha+\epsilon]$ are regular. It is known from the classical Morse theory that M_α is a strong deformation retract of $M_{\alpha+\epsilon}$. Therefore, $M_\alpha \cong M_{\alpha+\epsilon}$, hence $S(M_\alpha) \cong S(M_{\alpha+\epsilon})$. By the same argument, $(SM)_\alpha \cong (SM)_{\alpha+\epsilon}$. By the preceding construction, $S(M_{\alpha+\epsilon}) \cong (SM)_{\alpha+\epsilon}$. By transitivity, $S(M_\alpha) \cong (SM)_\alpha$. ■

Proof of Theorem 2.3 Equation (5) is a consequence of (1), Lemma 2.2, and the functoriality of the suspension operation. Equation (6) is an obvious consequence. Equation (8) follows from the fact that m_0 is the absolute minimum of the function at which a 0th order homological generator of infinite persistence is born. For proving Equation (7), the above arguments carry over to prove the commutativity of the diagram:

$$\begin{array}{ccc} H_0(M_\alpha) & \stackrel{H_0(j_f^{(\alpha,\beta)})}{\longrightarrow} & H_0(M_\beta) \\ \downarrow\cong & & \downarrow\cong \\ H_1(SM_\alpha)\oplus\mathbb{F} & \stackrel{H_1(j_{S_1 f}^{(\alpha,\beta)})}{\longrightarrow} & H_1(SM_\beta)\oplus\mathbb{F} \end{array}$$

To complete the proof, let $x_0, v_1, \ldots, v_n$ be representative vertices of a basis of H_0 homology generators for M_α, and $x_0, w_1, \ldots, w_m$ be those of a basis for M_β. We have

$$H_0(M_\alpha) = \oplus_{k=1}^{n}\mathbb{F}[v_k - x_0] \oplus \mathbb{F}[x_0] = \tilde{H}_0(M_\alpha) \oplus \mathbb{F}[x_0]$$

and the same holds true for $H_0(M_\beta)$ with respect to w_k's. The conclusion is reached by carrying the presented direct sum decomposition of the spaces to the isomorphisms shown by vertical arrows in the diagram and comparing their ranks.

Since ΣM_α is homotopy equivalent to SM_α for each α, the arguments carry over to $\Sigma_1 f$. ∎

Proof of Theorem 2.5 Equations (9) and (10) are direct corollaries, respectively, of (5) and (6). Now Equation (12) derives from (8), which signifies that the rank invariant function $\rho^0_{S_1 f}$ has a single cornerpoint (m_0, ∞). Similarly, $\rho^0_{S_1 g}$ has only one cornerpoint (n_0, ∞). It follows that $d(\rho^0_{S_1 f}, \rho^0_{S_1 g}) = |m_0 - n_0|$.

To prove Equation (11), see that from (7), the rank invariant functions ρ^0_f and $\rho^1_{S_1 f}$ differ only in that the former has one cornerpoint at infinity with the value m_0 which the latter does not have. Similarly, ρ^0_g has a cornerpoint (n_0, ∞) not present in $\rho^1_{S_1 g}$. Therefore, the computation of $d(\rho^1_{S_1 f}, \rho^1_{S_1 g})$ requires computing the bottleneck distance between two proper subsets of the points involved in the computation of $d(\rho^0_f, \rho^0_g)$. Equation (11) follows. However, in the case where $m_0 = n_0$, these two cornerpoints at infinity, differing by 0, will be matched in the optimal bijection between the sets of cornerpoints of ρ^0_f and ρ^0_g and will not influence the value of $d(\rho^0_f, \rho^0_g)$. From this, and Equations (10) and (12), (13) follows. ∎

Proof of Theorem 2.6 $D(\rho_{S_k\varphi}, \rho_{S_k\psi})$ is obtained as the supremum over admissible pairs of $d(\rho_{\mathrm{red}^{S_k\varphi}_{(\vec{l},\vec{b})}}, \rho_{\mathrm{red}^{S_k\psi}_{(\vec{l},\vec{b})}})$ (with the obvious change for the reduced rank invariants). Let us fix a particular pair $(\vec{l},\vec{b}) \in \mathrm{Adm}_k$. It is obvious from definitions that $\mathrm{red}^{S_k\varphi}_{(\vec{l},\vec{b})}(v) = S_1(\mathrm{red}^{\varphi}_{(\vec{l},\vec{b})})(v) = \mathrm{red}^{\varphi}_{(\vec{l},\vec{b})}(v)$ for all

$v \in \mathcal{V}(\mathcal{K})$. Now, $S_1(\mathrm{red}^{\varphi}_{(\vec{l},\vec{b})})(w_j) \geq \mathrm{red}^{S_k\varphi}_{(\vec{l},\vec{b})}(w_j) = \min_i l_i \max_i(m_{i,0} - b_i)/l_i$, $j = 0, 1$.

However, the appearance of w_0 and w_1 in the sublevel filtration for the function $\mathrm{red}^{S_k\varphi}_{(\vec{l},\vec{b})}$ before their appearance for the function $S_1(\mathrm{red}^{\varphi}_{(\vec{l},\vec{b})})$ does not affect their rank invariants of order 1 or greater, which will be identical. This along with Theorem 2.5 and the application of linear interpolation to $\mathrm{red}^{\varphi}_{(\vec{l},\vec{b})}$ and $\mathrm{red}^{\psi}_{(\vec{l},\vec{b})}$ allows us to show that

$$d(\tilde{\rho}^{q+1}_{\mathrm{red}^{S_k\varphi}_{(\vec{l},\vec{b})}}, \tilde{\rho}^{q+1}_{\mathrm{red}^{S_k\psi}_{(\vec{l},\vec{b})}}) = d(\tilde{\rho}^{q+1}_{S_1(\mathrm{red}^{\varphi}_{(\vec{l},\vec{b})})}, \tilde{\rho}^{q+1}_{S_1(\mathrm{red}^{\psi}_{(\vec{l},\vec{b})})}) = d(\tilde{\rho}^{q}_{\mathrm{red}^{\varphi}_{(\vec{l},\vec{b})}}, \tilde{\rho}^{q}_{\mathrm{red}^{\psi}_{(\vec{l},\vec{b})}}),\ q \geq 0,$$

$$d(\rho^{q+1}_{\mathrm{red}^{S_k\varphi}_{(\vec{l},\vec{b})}}, \rho^{q+1}_{\mathrm{red}^{S_k\psi}_{(\vec{l},\vec{b})}}) = d(\rho^{q+1}_{S_1(\mathrm{red}^{\varphi}_{(\vec{l},\vec{b})})}, \rho^{q+1}_{S_1(\mathrm{red}^{\psi}_{(\vec{l},\vec{b})})}) = d(\rho^{q}_{\mathrm{red}^{\varphi}_{(\vec{l},\vec{b})}}, \rho^{q}_{\mathrm{red}^{\psi}_{(\vec{l},\vec{b})}}),\ q \geq 1,$$

and

$$d(\rho^{1}_{\mathrm{red}^{S_k\varphi}_{(\vec{l},\vec{b})}}, \rho^{1}_{\mathrm{red}^{S_k\psi}_{(\vec{l},\vec{b})}}) = d(\rho^{1}_{S_1(\mathrm{red}^{\varphi}_{(\vec{l},\vec{b})})}, \rho^{1}_{S_1(\mathrm{red}^{\psi}_{(\vec{l},\vec{b})})}) \leq d(\rho^{0}_{\mathrm{red}^{\varphi}_{(\vec{l},\vec{b})}}, \rho^{0}_{\mathrm{red}^{\psi}_{(\vec{l},\vec{b})}}),$$

yielding Formulas (14), (15) and (16). ■

References

[1] M. Allili and D. Corriveau, Topological analysis of shapes using Morse theory, Computer Vision & Image Understanding, 105 (2007), 188–199.

[2] S. Biasotti, A. Cerri, P. Frosini, and D. Giorgi, A new algorithm for computing the 2-dimensional matching distance between size functions, Pattern Recognition Letters, 32 (2011), 1735–1746.

[3] S. Biasotti, A. Cerri, P. Frosini, D. Giorgi, and C. Landi, Multidimensional size functions for shape comparison, J. Math. Imaging Vision, 32(2) (2008), 161–179.

[4] G. Carlsson and A. Zomorodian. The theory of multidimensional persistence, Proc. of the 23rd annual Symposium on Computational Geometry, ACM New York 2007, 184-193.

[5] G. Carlsson, A. Zomorodian, A. Collins, and L. Guibas, Persistence Barcodes for Shapes, Proc. of the 2004 Eurographics/ACM SIGGRAPH symposium on Geometry processing, ACM, New Y 2004, 124–135.

[6] N. Cavazza, M. Ethier, P. Frosini, T. Kaczynski, and C. Landi, Comparison of persistent homologies for vector functions: from continuous to discrete and back, Comp. & Math. Appl., 66(4) (2013), 560–573.

[7] A. Cerri, B. Di Fabio, M. Ferri, P. Frosini, and C. Landi, Betti numbers in multidimensional persistent homology are stable functions, Mathematical Methods in the Applied Sciences, 36 (2013), 1543–1557.

[8] F. Christiansen, P. Cvitanovic, and V. Putkaradze, Spatiotemporal chaos in terms of unstable recurrent patterns, Nonlinearity, 10(1), (1997), 55–70.

[9] D. Cohen-Steiner, H. Edelsbrunner, J. Harer, Stability of persistence diagrams, Discrete & Comp. Geom., 37(1) (2007), 103–120.

[10] D. Cohen-Steiner, H. Edelsbrunner, J. Harer, Lipschitz Functions Have L_p-Stable Persistence, Foundations of Comput. Math., 10(2) 2010, 127–139.

[11] M. d'Amico, P. Frosini, and C. Landi, Using matching distance in size theory: a survey, Int. J. Imaging Syst. Technol., 16(5) (2006), 154–161.

[12] S. Day and W. D. Kalies, Rigorous computation of the global dynamics of integrodifference equations with smooth nonlinearities, SIAM J. Numerical Anal. to appear 2013.

[13] S. Derdar, M. Allili, and D. Ziou, Topological feature extraction using algebraic topology, Proc. SPIE-IS&T Electronic Imaging, Vision Geometry XV, (6499) (2007).

[14] H. Edelsbrunner and J. Harer, *Computational Topology. An Introduction*, Amer. Math. Soc. Providence 2009.

[15] P. Frosini, Measuring shapes by size functions, Proc. of SPIE, Intelligent Robots and Computer Vision X: Algorithms and Techniques, SPIE, 1607, Boston 1991, 122–133.

[16] M. Gameiro and J.-P. Lessard, Efficient rigorous numerics for higher-dimensional PDEs via one-dimensional estimates, SIAM J. on Num. Anal., 51(4) (2013), 2063–2087.

[17] M. Gameiro and M. Mischaikow, Topological characterization of spatial-temporal chaos, Phys. Rev. E 70, 035203(R) (2004).

[18] A. Hatcher, *Algebraic Topology*, Cambridge University Press 2002.

[19] T. Kaczynski, K. Mischaikow, and M. Mrozek, *Computational Homology*, Appl. Math. Sci. Series 157, Springer-Verlag, New York 2004.

[20] M. Mrozek, M. Żelawski, A.Gryglewski, S.Han, and A.Krajniak, Homological methods for extraction and analysis of linear features in multidimensional images, Pattern Rec., 45 (2012), 285–298.

[21] J.R. Munkres, *Elements of Algebraic Topology*, Addison-Wesley 1984.

[22] H. Sexton and M. Vejdemo Johansson. Plex: A system for computational homology. http://comptop.stanford.edu/u/programs/jplex/.

[23] A. Verri, C. Uras, P. Frosini, M. Ferri, On the use of size functions for shape analysis, Biol. Cybernet., 70(2) (1993), 99–107.

[24] A. Zomorodian and G. Carlsson, Computing Persistent Homology, Discrete & Comp. Geom., 33 (2005), 249–274.

Département de mathématiques
Université de Sherbrooke
2500, boul. de l'Université
Sherbrooke (Québec) J1K 2R1 Canada
{marc.ethier, t.kaczynski}@usherbrooke.ca

Institute of Computer Science
Uniwersytet Jagielloński
ul. Łojasiewicza 6
30-348 Kraków Poland